Monte Carlo study of the influence of antiferromagnetic exchange interactions on the phase transitions of ferromagnetic Ni-Mn-X alloys (X=In,Sn,Sb)

V. D. Buchelnikov,[1] P. Entel,[2] S. V. Taskaev,[1] V. V. Sokolovskiy,[1] A. Hucht,[2] M. Ogura,[3] H. Akai,[3] M. E. Gruner,[2] and S. K. Nayak[2]

[1]*Department of Condensed Matter Physics, Chelyabinsk State University, 454021 Chelyabinsk, Russia*

[2]*Department of Physics and Center for Nanointegration, CENIDE, University of Duisburg-Essen, 47048 Duisburg, Germany*

[3]*Department of Physics, Osaka University, 1-1 Machikaneyama, Toyonaka, Osaka 560-0043, Japan*

(Received 3 June 2008; revised manuscript received 29 September 2008; published 20 November 2008)

On the basis of Monte Carlo simulations using the Potts model Hamiltonian, we investigate the complex temperature dependence of magnetization of ferromagnetic Ni-Mn-X (X=In,Sn,Sb) Heusler alloys, in which part of the Mn atoms, which occupy the X sites, interacts antiferromagnetically with the Mn atoms on the Mn sublattice. It is shown that this antiferromagnetic exchange is responsible for metamagnetic behavior and a series of magnetic phase transitions in the Heusler alloys. For an optimal choice of parameters of the model Hamiltonian, which have partially been obtained from *ab initio* calculations, we are able to describe the physics associated with the coupled martensitic-magnetic phase transition. The simulations lead to a qualitative agreement with the experimental magnetization curves and their dependence on temperature and composition.

DOI: 10.1103/PhysRevB.78.184427 PACS number(s): 75.50.−y, 75.10.−b, 75.30.Sg

I. INTRODUCTION

In recent years, ferromagnetic (FM) Ni-Mn-X (X=Ga,In,Sn,Sb) Heusler alloys have attracted attention in view of their unique properties such as the shape memory effect, giant magnetocaloric effect (MCE), large magnetoresistance, and other interesting magnetic properties such as the coupled magnetic-martensitic transformation, i.e., the so-called magnetostructural phase transition.[1–9] For these alloys, the values of the MCE are comparable with those of the best magnetocaloric materials known so far, such as Gd-Si-Ge, La-Fe-Si, and Mn-As. The reason for the large MCE, i.e., large adiabatic temperature change ΔT in an external magnetic field, is closely related to the coupled magnetostructural phase transition, which exists in some off-stoichiometric FM Heusler systems over an extended range of compositions.[7–9] See also Ref. 10 for *new* information regarding the absolute value of ΔT for the $Ni_{2.19}Mn_{0.81}Ga$ alloy. The properties of magnetic Heusler alloys are of technological interest involving potential applications in actuator and magnetic refrigeration devices.

Recent experiments have shown that the structural phase transition from the paramagnetic (PM) cubic high-temperature austenite to FM tetragonal low-temperature martensite occurs with a steep slope as a function of the valence electron number per atom e/a,[11] which underlines the importance of the interplay of composition, band filling, and magnetic interactions in these alloys. From *ab initio* calculations of stoichiometric $Ni_{50}Mn_{25}X_{25}$ compounds it is known that the magnetic moments of nearest-neighbor Ni-Mn atoms (with Ni and Mn atoms on their regular sublattice sites) interact ferromagnetically; whereas the Mn-Mn interactions are predominantly FM but may have antiferromagnetic (AF) contributions depending on the distance of the Mn atoms. This means that even for the stoichiometric systems, the *ab initio* calculations reveal latent tendencies toward AF interactions which mostly involve the Mn-Mn interactions due to the long-range oscillatory behavior of the exchange interactions. This has been discussed in a series of papers dealing with *ab initio* calculations of magnetic exchange interaction parameters using different tools, see Refs. 12–17 and references therein. The magnetic interactions of Ni and Mn with the X atoms are usually small and negligible.[18] For the corresponding nonstoichiometric $Ni_{50}Mn_{25+x}X_{25-x}$ alloys, we have undertaken additional *ab initio* calculations[19,20] using the method in Ref. 21. These computations as well as results of recent experiments[9] highlight again that in the martensitic state, the Mn-excess atoms occupying the X-sublattice sites (X=In,Sb,Sn) interact with the Mn atoms on the Mn-sublattice sites antiferromagnetically. In particular, an enhancement of the AF interactions occurs at low temperatures. The AF interactions are also responsible for the drop in the thermomagnetization curves.[9,11,22,23]

Some results of our *ab initio* calculations regarding trends of the zero-temperature magnetic exchange coupling constants of stoichiometric Ni_2MnGa, Ni_2MnIn, and nonstoichiometric $Ni_{50}Mn_{34}In_{16}$ [$Ni_2Mn_{1.36}In_{0.64}$], respectively, using the Korringa-Kohn-Rostoker method in combination with the coherent potential approximation (KKR-CPA),[19,20] are presented in Fig. 1 and listed in Table I. The calculations have been done for the cubic structure in each case and also for the tetragonal structure in case of $Ni_{50}Mn_{34}In_{16}$. In the Monte Carlo simulations using the Heisenberg and Potts model, we will rely on these values.

Thus, we may conclude that in the martensitic phase of $Ni_{50}Mn_{25+x}X_{25-x}$, FM and AF interactions coexist and may also lead to competing FM and AF regions if the sample is inhomogeneous with respect to concentration [as is the case in $Ni_{50}Mn_{25+x}Sb_{25-x}$ for $10<x<16$ (Ref. 24)]. The consequence is that in these systems a sequence of phase transitions occurs, which are experimentally observed, from PM austenite to FM austenite and then to a mixed AF-FM martensitic state with decreasing temperature.[9,11,22,23] The resulting complex phase diagram in case of $Ni_{50}Mn_{25+x}Sb_{25-x}$ is shown in Fig. 2. Note that a theoretical phase diagram reproducing the different phases has already been obtained by us

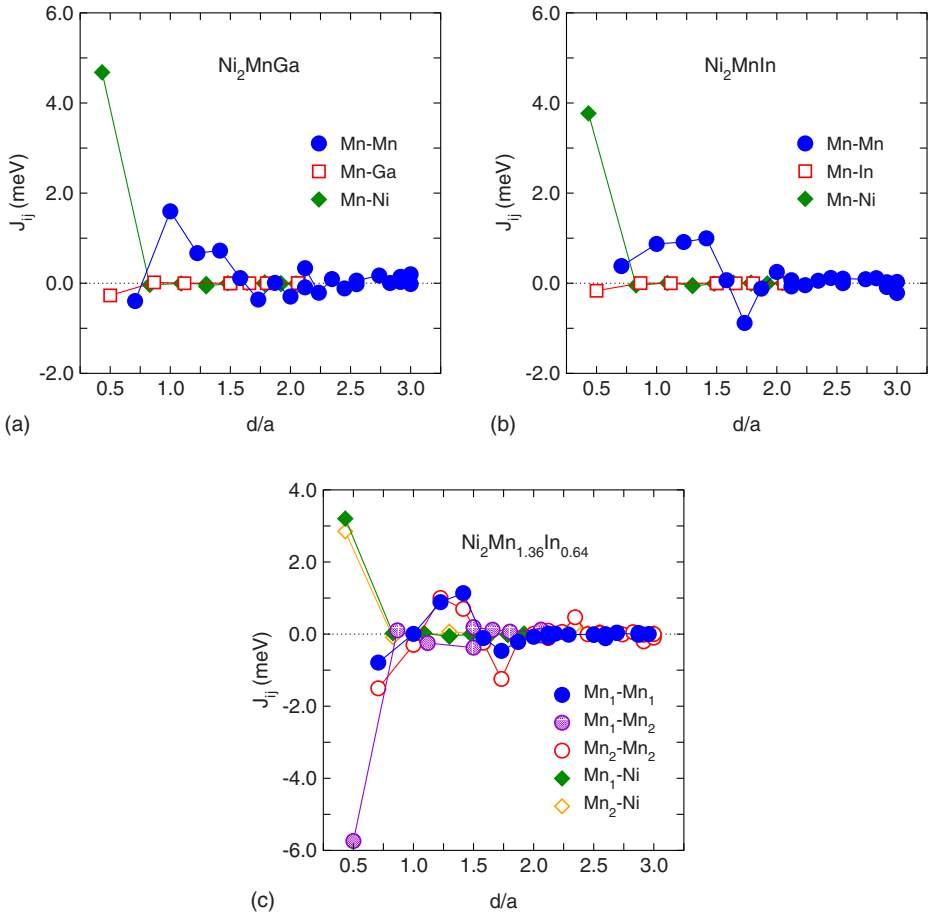

FIG. 1. (Color online) Top two panels: magnetic exchange interactions of the cubic phases of stoichiometric Ni_2MnGa and Ni_2MnIn as a function of the distance between the atoms (in units of the lattice constant). Lower panel: magnetic exchange interactions of nonstoichiometric cubic $Ni_{50}Mn_{34}In_{16}$ $[Ni_2Mn_{1.36}In_{0.64}]$. Mn-Mn, Mn-Ga, Mn-In, and Mn-Ni denote the magnetic interactions between the atoms on their respective sublattices. In the lower panel, the index 1 refers to Mn atoms on the Mn sublattice and index 2 to Mn atoms on the In sublattice, respectively.

using a phenomenological Ginzburg-Landau theory with Landau parameters taken from experiments where possible.[25,26]

From a theoretical point of view, it is a demanding task to try to obtain all phases in a self-consistent way. This would require the *ab initio* evaluation of *all* magnetic exchange parameters, i.e., for each composition, structure (austenite and martensite), and temperature and compare at each step of the calculation the corresponding free energies (consisting of internal energy contributions and entropic contributions from magnetic and phonon degrees of freedom with an underlying self-consistent determination of the temperature variation in the lattice constant). While this is possible for simple metals in reasonable computation time, for instance, see the work in Refs. 27 and 28, for the Heusler alloys, this is beyond our

TABLE I. Nearest-neighbor magnetic exchange interactions J_{ij} in meV of some cubic Ni-Mn-*X* Heusler systems. Mn_1 refers to Mn atoms on the original Mn sublattice; Mn_2 refers to Mn atoms on the *X* sublattice (Refs. 19 and 20).

J_{ij}	Ni_2MnGa	Ni_2MnIn	$Ni_{50}Mn_{34}In_{16}$
Mn_1-Mn_1	−0.41	0.41	−0.83
Mn_1-Mn_2			−5.74
Mn_2-Mn_2			−1.48
Mn_1-Ni	4.67	3.74	3.19
Mn_2-Ni			2.82

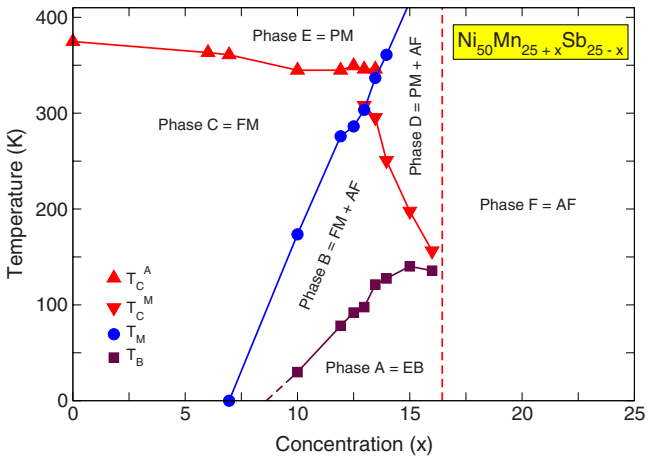

FIG. 2. (Color online) Temperature-composition (*T*-*x*) phase diagram showing the six different magnetic regions of $Ni_{50}Mn_{25+x}Sb_{25-x}$ (figure adapted from Ref. 24). Phase A is the exchange bias (EB) region where FM and AF regions exist in the system. Phase B is the martensitic region with coexistence of both FM and AF orderings. Phase C is the FM austenitic phase. Phase D is the PM and AF phases. Phase E is the PM austenitic phase and phase F denotes the AF phase. Labels *A* and *M* at T_C refer to the Curie temperatures in the austenitic (triangles up) and martensitic (triangles down) regions, respectively. Filled (blue) circles mark the martensitic transformation. See Ref. 24 for more details.

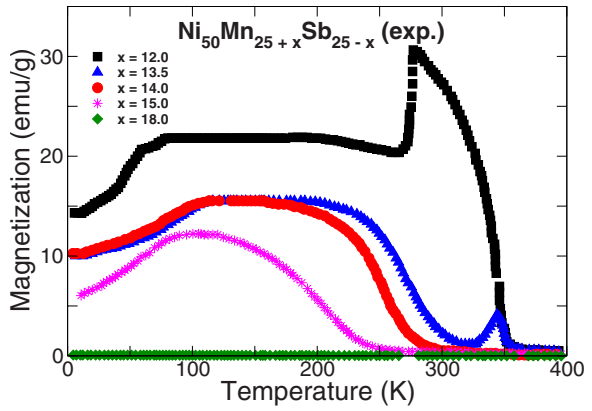

FIG. 3. (Color online) Experimental variation in magnetization of $Ni_{50}Mn_{25+x}Sb_{25-x}$ as a function of temperature for different compositions. The data have been taken from Ref. 24.

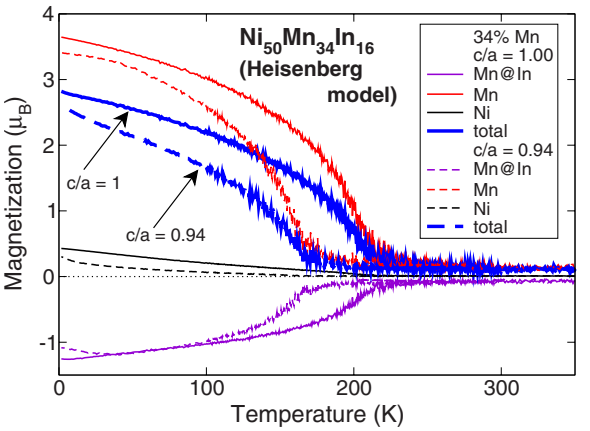

FIG. 4. (Color online) Variation in the individual magnetic moments of Mn_1, Mn_2, and Ni atoms of $Ni_{50}Mn_{34}In_{16}$ (per volume or formula unit) alloy as a function of temperature as obtained from Monte Carlo simulations for the classical Heisenberg model. The solid lines represent magnetic behavior in the cubic (austenitic) structure ($c/a=1$), and the dashed lines show the temperature dependence of spin moments for the tetragonal (martensitic) structure ($c/a=0.94$).

computational facilities and beyond the purpose of the present paper.

The purpose of this paper is to present a unified description of structural martensitic and associated first-order magnetic phase transitions (magnetostructural transitions) by using a model Hamiltonian as simple as possible, which, however, would allow to explore the richness of the phase diagram for small compositional changes as, for instance, displayed by the phase diagram of $Ni_{50}Mn_{25+x}Sb_{25-x}$ shown in Fig. 2.[24] The temperature variation in the corresponding magnetization curves for fixed concentrations x in Fig. 3 shows how subtle changes in composition lead to drastic changes in the behavior of $M(T)$.

Therefore, in this paper, we have chosen a *q-state* Potts model[29,30] Monte Carlo method to simulate the magnetic interactions and have extended this method by incorporating the Blume-Emery-Griffiths (BEG) (Refs. 31) model in order to simultaneously allow for a structural transformation from the cubic to tetragonal lattice as well as retaining two martensitic tetragonal variants in the martensitic phase. The model parameters have been chosen such that, for example, the important AF Mn_1-Mn_2 interaction is of the order of the value listed in Table I with slight changes for the different alloys considered; the energy changes associated with the structural changes are also not too far off when compared to *ab initio* total-energy differences.

In order to demonstrate the important role of the q-state Potts model—employed in this paper—for the simulation of first-order magnetic phase transitions seen in the experiments, we show in Fig. 4 results of Monte Carlo simulations using the classical Heisenberg model with *ab initio* exchange parameters for the cubic ($c/a=1$) and tetragonal ($c/a=0.94$) phases of $Ni_{50}Mn_{34}In_{16}$. There are two important observations. First, the simulations yield Curie temperatures which approximately agree with the experimental ones[32] for the austenitic ($c/a=1$) and martensitic ($c/a=0.94$) phases, respectively (see also Fig. 5). Second, for the composition $Ni_{50}Mn_{34}In_{16}$, the alloy is on the edge of a transformation from the cubic to the martensitic structure. Figure 4 shows that the magnetic moments of Mn and Ni decrease continuously and smoothly for both phases with increasing temperature, which is typical for a second-order-like phase transition, in spite of the fact of having competing FM and AF *ab initio* exchange interactions. Thus, without adding further terms to the Hamiltonian and without reformulating the magnetic interactions of the model Hamiltonian, the Monte Carlo simulations using the simple Heisenberg Hamiltonian do not reproduce the strong increase in the magnetization at the Curie

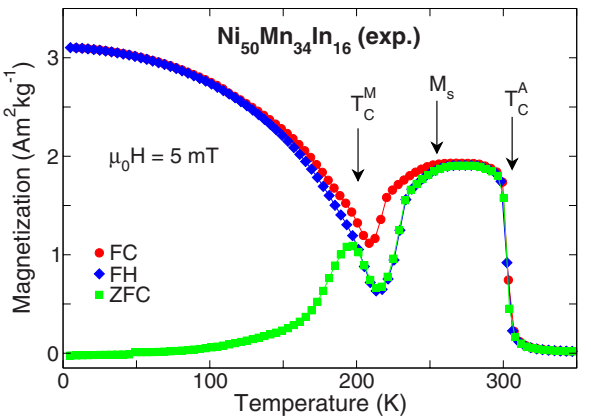

FIG. 5. (Color online) Field-cooled (FC), field-heated (FH), and zero-field-cooled (ZFC) experimental magnetization curves of $Ni_{50}Mn_{34}In_{16}$ (in an external magnetic field of $\mu_0 H=5$ mT). The arrows mark the Curie temperature in the austenitic phase $T_C^A=300$ K, the martensitic start temperature $M_s=264$ K, and the Curie temperature in the martensitic phase $T_C^M=200$ K, respectively. Note that the FC and FH $M(T)$ curves in the martensitic phase qualitatively agree with $M(T)$ for $c/a=0.94$ of the Heisenberg model in Fig. 4. The strong increase in $M(T)$ in the austenitic phase below T_C^A cannot be reproduced by the Heisenberg model, which lacks the information of the detailed magnetic behavior of the polycrystalline sample as well as the information about the change in the magnetic exchange parameters with change in the lattice parameters of the martensitic phase when decreasing the temperature below T_C^A. The figure has been adapted from Ref. 32.

temperature for the PM→FM transition with decreasing temperature nor the decrease (drop) in the magnetization when further decreasing the temperature near the structural transition temperature from FM austenite to mixed AF-FM martensite, as observed experimentally. This means that the simple classical Heisenberg model without additional terms cannot account for the richness of the phase diagram. The advantage of choosing the q-state Potts model compared to the classical Heisenberg model is that the former allows first-order phase transitions for $q \geq 4$, and, as discussed in Sec. II, the refined q-state Potts model, in addition, allows to describe the magnetostructural phase transition as well.

For the merit of work done by using an effective Heisenberg model for the description of magnetocaloric properties of rare-earth-based compounds and Heusler systems, we refer to Refs. 33–38. In addition to this model, which allows only a magnetic transition of second order (as shown in Fig. 4) without taking into account the structural transformation, other work exists as in Ref. 39, where the model has been extended to describe the premartensitic phase transformation in stoichiometric Ni_2MnGa. In this two-dimensional model, interaction between structural and magnetic degrees of freedom was included by using the Ising model and the degenerated three-state BEG model. Our model employed here goes beyond this ansatz.

Another question is whether the physical properties of Ni-Mn-X would require to consider also the softening of phonons associated with premartensitic or martensitic transformation observed in some of the alloys close to stoichiometric composition.[40–42] In most pronounced cases, the phonon softening involves energy changes in the order of 1–2 meV. In the BEG model,[39] the authors assumed that the structural part of the exchange constant is proportional to the soft phonon energy at the phase-transition temperature. In our Monte Carlo simulation of magnetic properties of Ni-Mn-X using an extended BEG model, which allows for coupled magnetostructural phase transitions from FM austenite to mixed AF-FM martensite and magnetic phase transitions from PM to FM austenite, the same order of energies is taken into account as in Ref. 39. An explicit calculation of the phonon softening for the off-stoichiometric Heusler systems is not undertaken; this is beyond the goals of the present paper.

II. THEORETICAL MODEL

In the presence of a structural phase transformation, the martensitic phase may exhibit several variants, i.e., existence of degenerate phases. These variants can be described by lattice distortions (compression or expansion) during the phase transition along the x, y, and z axes, which for the cubic phase yields six structural variants. The high-temperature phase corresponds to a phase with vanishing displacements, i.e., $x=y=z=0$. Thus, during cooling, the austenitic phase may choose any of the six variants. In our model, we consider only two variants of martensite with lattice deformation along $\pm x$ or $\pm y$ or $\pm z$ axes, i.e., a double-degenerated cubic phase.

In the model defined below, we use a simple three-dimensional cubic lattice with periodic boundary conditions. Although the magnetic interactions between the Ni-Mn and X-Mn atoms are nonzero, for the sake of simplicity, we consider a renormalized effective spin model involving only the interactions between the magnetic moments of the Mn atoms and neglect the contributions from the Ni and X atoms.

Thus, in our effective model we consider all lattice sites to be occupied by magnetic Mn atoms. In case of stoichiometric Ni_2MnX samples, all Mn atoms are taken to interact with each other ferromagnetically. For the nonstoichiometric cases $Ni_2Mn_{1+x}X_{1-x}$ $(x \neq 0)$, we assume that a fraction of the Mn atoms on the simple-cubic lattice (corresponding to the composition of the real sample) interacts with each other and the other Mn atoms antiferromagnetically, whereby the initial configuration of these Mn atoms is randomly chosen.

Regarding the magnetic interactions, we consider only nearest-neighbor interactions (although the *ab initio* exchange coupling constants show long-range oscillatory behavior[20]). Then, the Hamiltonian describing the system can be represented by two interacting contributions: one that describes the magnetic interactions and the other one taking care of the structural distortion. As pointed out, for the magnetic part, we have chosen the q-state Potts model which allows to simulate the magnetic phase transition from the FM to PM phase.[43] Here, q is the number of spin states. In case of $q=2$, the q-state Potts model is identical with the Ising model. In our case, we consider a three-dimensional model with five spin states due to the fact that in Ni-Mn-X, the spin state of Mn corresponds to $S=4/2$ with $2S+1$ possible spin projections, which we describe by the *five-state* Potts model.

The structural part is described by the degenerated three-state BEG model allowing for a structural transformation from the cubic (austenitic) phase to the tetragonal (martensitic) phase.[39] In the original BEG model, the cubic phase has a degeneracy of only one; in our model we have a twofold degeneracy.

The corresponding Hamiltonian (1) consists of three contributions, the magnetic part is described by Eq. (2), the elastic part by Eq. (3), and the magnetoelastic interaction is defined in Eq. (4),

$$\mathcal{H}^* = \mathcal{H}_m^* + \mathcal{H}_{\mathrm{el}}^* + \mathcal{H}_{\mathrm{int}}^*, \tag{1}$$

$$\mathcal{H}_m^* = -J_{\mathrm{fm}}^* \sum_{\langle ij \rangle} \delta_{S_i,S_j} - J_{\mathrm{afm}}^* \frac{T^* - T_{\mathrm{afm}}^*}{T_{\mathrm{afm}}^*} \sum_{\langle ij \rangle} \delta_{S_i,S_j} - h^* \sum_i \delta_{S_i,S_g}, \tag{2}$$

$$\mathcal{H}_{\mathrm{el}}^* = -\sum_{\langle ij \rangle} \sigma_i \sigma_j - K^* \sum_{\langle ij \rangle} (1-\sigma_i^2)(1-\sigma_j^2) - zT^* \ln(p) \sum_i (1-\sigma_i^2), \tag{3}$$

$$\mathcal{H}_{\mathrm{int}}^* = 2U^* \sum_{\langle ij \rangle} \delta_{S_i,S_j} \left(\frac{1}{2} - \sigma_i^2\right)\left(\frac{1}{2} - \sigma_j^2\right) - \frac{1}{2} U^* \sum_{\langle ij \rangle} \delta_{S_i,S_j}. \tag{4}$$

Here, the stars indicate that the Hamiltonian contains only renormalized parameter values defined by ratios over J (J is

chosen such that the magnetic exchange interactions are of the order of the calculated *ab initio* parameters), which is the energy scale of the first term in Eq. (3) for the tetragonal distortion, so, $\mathcal{H}^*=\mathcal{H}/J$, etc.

$$J_{\mathrm{fm}}^* = \frac{J_{\mathrm{fm}}}{J}, \quad K^* = \frac{K}{J},$$

$$J_{\mathrm{afm}}^* = \frac{J_{\mathrm{afm}}}{J}, \quad T^* = \frac{k_B T}{zJ},$$

$$h^* = \frac{g\mu_B H_{\mathrm{ext}}}{J}, \quad T_{\mathrm{afm}}^* = \frac{k_B T_{\mathrm{afm}}}{zJ},$$

$$U^* = \frac{U}{J},$$

where J_{fm} and J_{afm} are the FM and AF exchange constants, respectively; T is the actual temperature and T_{afm} is the temperature at which the AF interaction changes its sign in the second term in Eq. (2); z is the coordination number of a given site; δ_{S_i,S_j} is the Kronecker symbol which limits the spin-spin interaction to interactions between the same q state only (we have adopted the notation in Ref. 44 for the spin-spin interactions) and the sum is over nearest neighbors; S_g is a kind of a *ghost spin*, whose direction is that of the external magnetic field, a spin parallel to the ghost spin is favored by positive H_{ext}, see Ref. 44; J and K are the *exchange constants* of the structural Hamiltonian (3), where p is the degeneracy factor and U in Eq. (4) is the strength of the magnetoelastic interaction; finally, g is the Landé factor, μ_B is Bohr's magneton, and k_B is the Boltzmann constant. The variable $\sigma_i=1$, 0, and -1 represents the deformation state at each site, where $\sigma_i=0$ denotes the undistorted phase and $\sigma_i=\pm 1$ the distorted phases. The coordination number z is six, since we do not consider the Ni and X atoms explicitly. Thus the model can be considered as the simplest model to account for the existence of metamagnetic states and associated first-order-like magnetic phase transitions. Depending on the parameters, the martensitic transformation accompanying the increase in AF interactions below T_{afm} can also be a first-order-like transition. At least, this guarantees the occurrence of a combined magnetostructural transition.

As stated above, we consider a three-dimensional cubic lattice. All sites of the lattice are occupied by magnetic Mn atoms. For stoichiometric Ni_2MnX, all Mn atoms interact FM with each other; while for nonstoichiometric $Ni_2Mn_{1+x}X_{1-x}$, a fraction of Mn atoms on this lattice interacts AF with each other and the remaining Mn atoms. The initial configuration of these Mn atoms has been chosen randomly with the total number determined from the experimental compositions. The remaining Mn spins interact ferromagnetically as for the stoichiometric case. This is modeled by Eq. (2). In addition, Eq. (2) contains a magnetic-field term.

The AF interaction term in Eq. (2) limits the AF interactions to the low-temperature phase. For $T>T_{\mathrm{afm}}$, i.e., $T^*>T_{\mathrm{afm}}^*$, this interaction term will change sign resulting in additional FM interactions. Accordingly, above this temperature, enhanced FM interaction between all Mn atoms occurs. Since this means that there will be no transition from FM austenite to PM austenite, we allow the maximal value of the factor $(T^*-T_{\mathrm{afm}}^*)/T_{\mathrm{afm}}^*$ to be in unity, i.e., for temperatures $T^*>2T_{\mathrm{afm}}^*$ the prefactor of the second term in Eq. (2) is assumed not to depend on temperature any more and is set equal to $-J_{\mathrm{afm}}^*$. By this, we achieve simultaneous magnetic and martensitic phase transitions. Moreover, the Hamiltonian may lead to several magnetic phase transitions from the high-temperature PM phase to different magneto-ordered phases with decreasing temperature such as the FM and AF phases or mixed FM and AF phases. The critical temperatures will in each case be determined by the degree of competition between FM and AF interactions depending on the strengths of exchange coupling constants.

With respect to the elastic part of the Hamiltonian (3), the first term characterizes the interaction between single strains σ_i in the tetragonal (martensitic) phase. The second term defines the interaction between single strains σ_i in the cubic (austenitic) phase. Large values of K^* will stabilize the pure cubic phase in which $\sigma_i=0$ holds. Moreover, the parameter K^* and the degeneracy p of the zero state control the order of the transition, which changes from second order (for low values of K^*) to first order. In case of low values of K^*, the cubic phase will be stabilized in the high-temperature region where we find an equal population of the strain variables $\sigma_i=0$ and ± 1.[39] The last term in Eq. (3) characterizes a temperature-dependent degeneracy factor p for the cubic phase or, in other words, this term defines a temperature-dependent crystal field.[45] As in the work of Ref. 39, the Hamiltonian (3) describes the transition from the high-temperature cubic (austenitic) phase to the low-temperature tetragonal (martensitic) phase with decreasing temperature where the transition temperature is determined by K^*. Taking into account the magnetoelastic part (4) of the Hamiltonian allows not only for a structural phase transition to the martensitic phase (tetragonal phase with strains $\sigma_i=+1$ or -1) but also allows to describe the premartensitic phase (*average cubic phase* with equal parts of strains $\sigma_i=\pm 1$ and 0.[39])

To summarize, the extended Potts model Hamiltonian in Eqs. (1)–(4) allows to describe the different structural, magnetic, as well as the coupled magnetostructural phase transitions as they are observed in experiments. In order to calculate the mean energy for a given temperature, we use the same algorithm as in Ref. 46: (a) Generate the initial spin configuration (the ferromagnetically ordered state) and the initial strain configuration (the tetragonal state, one of the martensitic variants). Calculate the energy of the initial configuration H_1 according to Eq. (1). (b) Select a particular site i and randomly change the values of the spin state q and strain σ_i. (c) Calculate the energy for this new configuration (H_2) according to Eq. (1). (d) If $H_2<H_1$, accept the new configuration with energy H_2 and go to step (h). (e) If $H_2>H_1$, calculate the probability factor $\exp(-\Delta\mathcal{H}/k_BT)$. (f) Generate a random number r such that $0<r<1$. (g) If $r<\exp(-\Delta\mathcal{H}/k_BT)$, accept the new configuration with energy H_2, else preserve the old configuration of spin and strain and return to step (b). (h) Move to the next site, change at random the values of the spin state q and deformation σ_i, and return to step (c). (i) Repeat the entire process until all the lattice sites are swept. The whole process of the partition of

TABLE II. Model parameters for the Heusler alloys Ni-Mn-X (X=In,Sn,Sb) in meV used in the Monte Carlo simulations for the extended Potts model defined in Eqs. (1)–(4).

	J	J_{fm}	J_{afm}	U	K	T_{afm}
$Ni_{50}Mn_{35}Sn_{15}$	1.35	3.1	3.24	−0.135	−0.135	1.89
$Ni_{50}Mn_{37.5}Sb_{12.5}$	1.67	4.68	3.67	−0.835	−0.167	2.37
$Ni_{50}Mn_{34.95}In_{15.05}$	1.58	3.16	3.48	−0.32	−0.24	2.26
$Ni_{45}Co_5Mn_{36.6}In_{13.4}$	1.68	0	4.03	−0.588	−0.84	2.37

the lattice is described by one Monte Carlo step. For a given temperature, the mean energy $\langle H\rangle$ and mean-squared energy $\langle H^2\rangle$ are calculated by using

$$\langle \mathcal{H}^*\rangle = \frac{1}{N_c - N_0}\sum_{i>N_0}^{N_c} \mathcal{H}_i^*,$$

$$\langle \mathcal{H}^{*2}\rangle = \frac{1}{N_c - N_0}\sum_{i>N_0}^{N_c} \mathcal{H}_i^{*2}, \tag{5}$$

where N_c is the total number of Monte Carlo steps, N_0 is the number of Monte Carlo steps which are used for the thermalization; the index i denotes the Monte Carlo step.

In the q-state Potts model, the process of calculating the magnetization of the whole system per Monte Carlo step differs from the case of the Ising model. As is well known, for the Ising model for one Monte Carlo step, the spin average is calculated by summing over all spins throughout the lattice. For the q-state Potts model for one Monte Carlo step, it is necessary to calculate the maximal number of sites on the lattice having the similar magnetic state $N_{\max}$. Thus, the mean value of $N_{\max}$ is calculated by summing the averages of all Monte Carlo steps,

$$\langle N_{\max}\rangle = \frac{1}{N_c - N_0}\sum_{i>N_0}^{N_c} \langle N_{\max}\rangle_i. \tag{6}$$

Then, for the q-state Potts model, the magnetization of the system at a given temperature is calculated by

$$m = \frac{1}{L^3}\frac{qN_{\max} - N_{\mathrm{mag}}L^3}{q-1}, \tag{7}$$

where L is the linear size of the system (L^3=N), q is the number of magnetic states, $N_{\max}$ is the maximal number of same magnetic states on the lattice, and N_{mag} is the number of magnetic atoms.

As in the BEG model used in Ref. 39, we define the strain order parameter in the following way:

$$\varepsilon = \frac{1}{N}\sum_{1}^{N} \sigma_i. \tag{8}$$

For the degenerate BEG model, we have two cubic states in which the parameter ε is equal to zero. For the first cubic state, we have equal population of strain variables σ_i=0 and $\pm$1. This case corresponds to an average cubic phase, which we define as premartensitic phase. The second state is a pure cubic phase in which we have σ_i=0. For ε=1, we find the tetragonal phase for one of the variants σ_i=1 or −1.

With respect to material parameters, the magnetic part of the specific heat and susceptibilities associated with fluctuations of the order parameters have yet to be calculated, but may be obtained from

$$C_{\mathrm{mag}}^*(T^*,h^*) = \frac{1}{N}\frac{\langle \mathcal{H}^{*2}\rangle - \langle \mathcal{H}^*\rangle^2}{T^{*2}}, \tag{9}$$

$$\chi_m(T^*,h^*) = \frac{\langle m^2\rangle - \langle m\rangle^2}{T^*}, \tag{10}$$

$$\chi_\varepsilon(T^*,h^*) = \frac{\langle \varepsilon^2\rangle - \langle \varepsilon\rangle^2}{T^*}. \tag{11}$$

III. NUMERICAL RESULTS FOR MAGNETIC HEUSLER ALLOYS

In the following, we discuss numerical results for Ni-Mn-X alloys obtained by Monte Carlo simulations using the extended Potts model. The corresponding equilibrium simulations have been carried out using the standard Metropolis algorithm. Changes in the *spin states* q and σ_i are treated independently and are accepted or rejected according to the single-site transition probability W=min{1, $\exp(-\Delta\mathcal{H}^*/T^*)$}. For the simulations of the three-dimensional cubic lattice, we used periodic boundary conditions and six nearest neighbors for each site. The number of sites in the lattice was taken to be N=15^3. The distribution of the Mn atoms with AF interactions is chosen at random but its total number is determined from the experimental composition of Ni-Mn-X. The time unit is one Monte Carlo step, which consists of N attempts to change the q and σ_i variables. For a given temperature, the number of Monte Carlo steps at each site varies between 10^5 and 10^6. We start the Monte Carlo simulations from the FM martensite phase with q=2 and σ_i=1. The various quantities are averaged over 400 configurations, each taken after every 100 Monte Carlo steps and discarding the first 10^4 Monte Carlo steps for equilibration. The degeneracy factor was taken as p=2, Landé factor was taken as g=2, and the number of q states was equal to 5. In order to find the spin state at each lattice site, we choose a random number r such that $0<r<1$ and fix the value of q according to the scheme: if $0\le r\le n/5$ then q=n where n =1…5.

In the Monte Carlo simulations we adopted the parameter values listed in Table II in order to describe the magnetic and

structural properties of Ni-Mn-X alloys in an optimal way. As explained, all model parameters are renormalized parameter values defined by ratios over the structural exchange constant J with $J>0$. The actual values of the model parameters used in the simulations have been chosen in the following way. The information about the approximate value of the structural exchange interaction was taken from experimental data of the phonon-dispersion curves of Ni-Mn-Ga alloys.[40,42] As is known from Ref. 42, the exchange constant J is proportional to the energy of the soft phonon and for Ni-Mn-Ga with $T_m \approx 284$ K, $T_C \approx 364$ K the value of J at the phase-transition temperature is of the order of 2 meV. Note that this value of the exchange constant J can be obtained from the Monte Carlo calculations of the reduced martensitic transition temperature T_m^*. According to the Monte Carlo calculations in Ref. 39, the reduced temperature in martensitic transition T_m^* in Ni-Mn-Ga is ≈ 2.25. Taking into account the experimental value for the martensitic transition temperature of Ni-Mn-Ga from Ref. 42, $T_m \approx 284$ K, we find for the lattice exchange constant $J=k_B T_m / z T_m^* \approx 2.7$ meV for $z=4$.

For estimating the values of J for the different alloys in Table II, we used the same method: for each alloy, we determined the reduced temperature T_m^* in the martensitic transition from the Monte Carlo simulations. From this, we obtained the ratio T_m / T_m^*, where T_m is the experimental martensitic transition temperature for each alloy. (So, the experimental value of T_m for each system is used as a fit parameter.) Finally we determine the lattice exchange constant J by using $J=k_B T_m / z T_m^*$ with $z=6$ for the cubic lattice. The calculated exchange constants J for different alloys are listed in Table II. The knowledge of J allows us to express the different parameters values in meV, which are also given in Table II. As can be seen, these values nearly coincide with values obtained for the magnetic interactions by *ab initio* calculations.[20] Furthermore, in order to determine K^*, which characterizes the martensitic transition, and the value of the magnetoelastic interaction U^*, we have used the following conditions: $J_{\mathrm{fm}}^* > 0$, $J_{\mathrm{afm}}^* > 0$, $U^* < 0$, $J_{\mathrm{fm}}^* + U^* > 0$, and $K^* < 0$.[39] In this context, we would like to note that for an appropriate value of K^* with $K^* > 0$ (in the BEG model) three phase transitions are possible with increasing temperature: the martensitic transition from the tetragonal phase to the quasicubic one, the premartensitic transition from the quasicubic phase to the cubic one at T_I, and the magnetic transition from the FM phase to the PM one with a sequence of transitions as $T_m^* < T_I^* < T_C^*$.[39] Since the premartensitic transition in Ni-Mn-X alloys has not been observed experimentally, we simply choose $K^* < 0$. In the simulations, we fix the value of the FM and AF interactions, while for the difference between T_m^* and T_C^*, we have used different values of U^*, K^*, and T_{afm}^* for the different alloys under consideration.

Computational results are presented in Figs. 6–8. In Fig. 6, the top panel shows the simulations results while the lower panel presents the experimental data taken from Ref. 22 for $Ni_{50}Mn_{35}Sn_{15}$ in an external magnetic field of 0.01 T. The simulations reproduce the experimental trends and yield two phase transitions at ≈ 320 K ($T^* \approx 3.4$) and ≈ 183 K ($T^* \approx 1.95$), respectively. The first transition is from PM cubic austenite to FM cubic austenite, the second transition is the coupled magnetostructural phase transition from FM cubic austenite to mixed FM-AF tetragonal martensite. The behavior of the strain order parameter ε shows the onset of the structural phase deformation at ≈ 183 K ($T^* \approx 1.95$). This transition is also accompanied by a change in sign of the exchange integral from FM to AF interaction; see second term in Eq. (2). For temperatures below the structural transition, the corresponding term describes AF interactions. In the martensitic state, the concentration of Mn atoms which interact antiferromagnetically with each other and with the remaining Mn atoms is 40%. In the austenitic phase, these 40% of Mn atoms begins to interact ferromagnetically with each other and with the remaining Mn atoms.

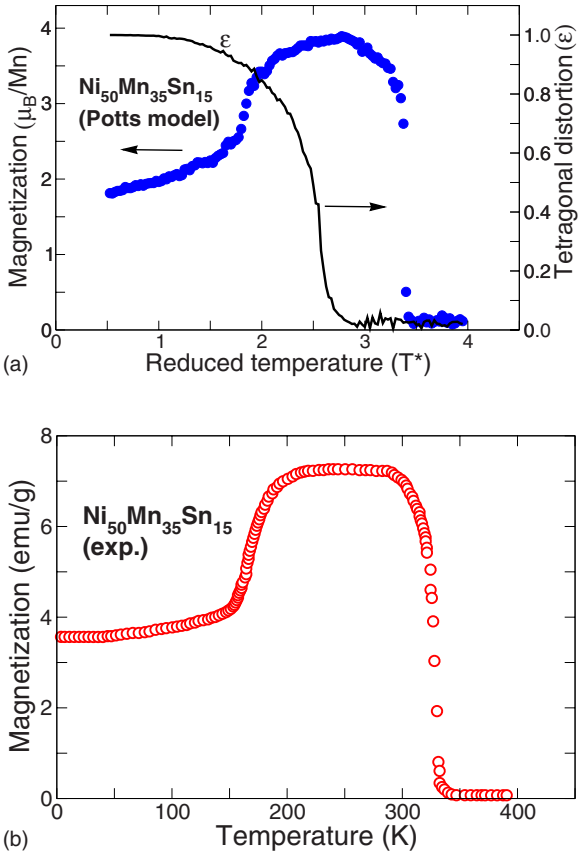

FIG. 6. (Color online) Top panel: magnetization in units of μ_B/atom and tetragonal distortion ε as a function of the reduced temperature $T^*=k_B T/(zJ)$ obtained by Potts model Monte Carlo simulations for $Ni_{50}Mn_{35}Sn_{15}$. Magnetization and strain are marked by filled (blue) circles and solid line, respectively. Lower panel: experimental temperature dependence of magnetization taken from Ref. 22.

Figure 7 shows the magnetization and the strain as a function of reduced temperature for $Ni_{50}Mn_{37.5}Sb_{12.5}$ in the absence of a magnetic field. The two magnetic phase transitions are now at $T^* \approx 3.07$ and at $T^* \approx 2.45$, respectively. We obtain from the simulations a PM-FM transition in the cubic state at $T^* \approx 3.07$. The second transition at $T^* \approx 2.45$ describes the FM to mixed FM-AF phase transition which is again accompanied by a tetragonal transformation. The decrease in magnetization in the martensitic state results again from the influence of the AF exchange interactions. Figure 7 shows also the experimental values taken from Ref. 23.

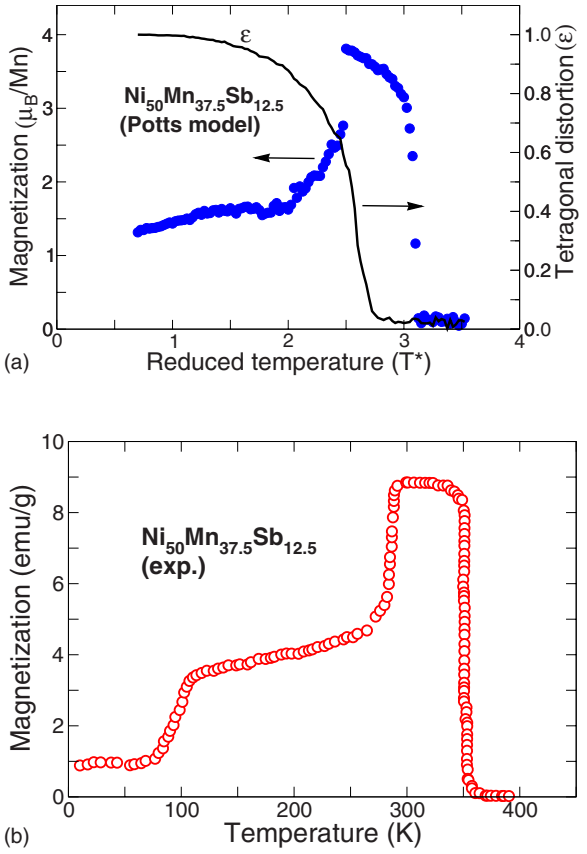

FIG. 7. (Color online) Top panel: Potts model simulation results showing the variation in magnetization (circles) and strain (tetragonal distortion, solid line) as a function of reduced temperature T^* for $Ni_{50}Mn_{37.5}Sb_{12.5}$. Lower panel: experimental temperature dependence of magnetization taken from Ref. 23.

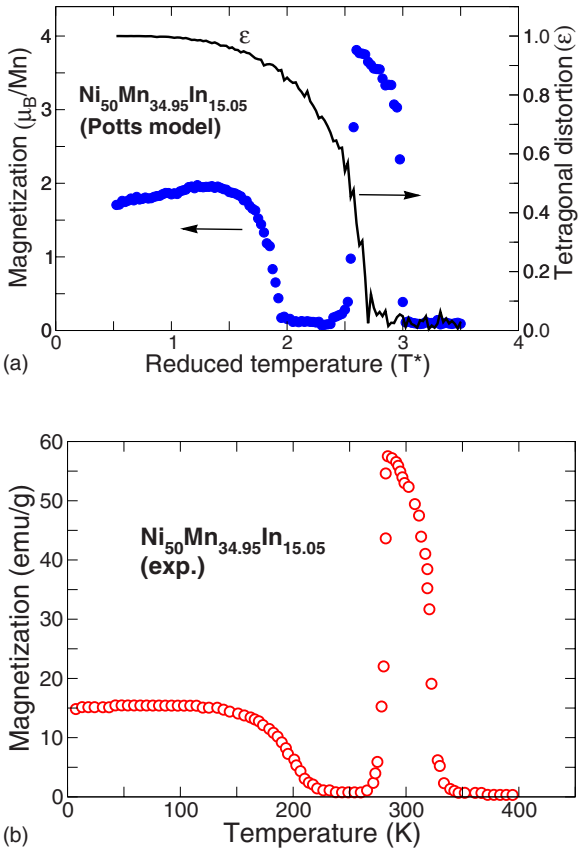

FIG. 8. (Color online) Top panel: results of Potts model Monte Carlo simulations of magnetization (circles) and strain (tetragonal distortion, solid line) as a function of the reduce temperature T^* for $Ni_{50}Mn_{34.95}In_{15.05}$. Lower panel: experimental results taken from Ref. 47.

In Fig. 8, we show theoretical and experimental results for $Ni_{50}Mn_{34.95}In_{15.05}$ for the case of an external magnetic field of 0.1 T. We observe here three phase transitions at 330 ($T^* \approx 3.0$), 280 ($T^* \approx 2.55$), and 200 K ($T^* \approx 1.82$), respectively. At 330 K ($T^* \approx 3.0$), we find the PM-FM transition in the cubic state. The second transition is the structural transition from the FM cubic state to the PM or AF tetragonal phase. The third transition is the magnetic phase transition in the tetragonal state. The decrease in magnetization in the low-temperature FM martensitic state is again the influence of AF exchange on the FM spin system. The experimental data in Fig. 8 have been taken from Ref. 47.

For application in refrigeration devices, higher transition temperatures are needed and intense research is going on to find new magnetic Heusler alloys allowing for the construction of shape memory or refrigeration devices at temperatures higher than room temperature. One possibility to obtain higher transition temperatures is to insert magnetic transition metal or rare-earth ions with a large spin moments to achieve higher working temperatures. Figure 9 shows simulations results for the case that 5 at. % Ni have been replaced by Co, whereby the experimental data have been taken from Ref. 6.

We note that an additional effect is associated when incorporating Co. It is known from experimental studies that adding Co to Ni-Mn-In will lead to the disappearance of the FM phase and the onset of AF in the low-temperature martensitic phase. In Fig. 9, we can observe two phase transitions at 380 ($T^* \approx 3.26$) and 300 K ($T^* \approx 2.57$), respectively. The first transition is the magnetic transition from the cubic PM state to the cubic FM one. The second transition is associated with the coupled magnetostructural transition from the cubic FM state to the tetragonal AF one. Since the martensitic phase is now AF ordered, we have switched off the FM interaction, i.e., the first term in Eq. (2), in the Monte Carlo simulations.

Although, we have chosen parameters for the effective Hamiltonian which partially rely on *ab initio* calculations, small variations in the parameters were chosen such that the experimental results were reproduced in an optimal way. The general agreement with experiment with respect to the reproduction of two first-order phase transitions shows that the model seems to contain indeed the essential terms in order to describe the magnetic Heusler alloys over the entire phase diagram.

In order to test the predictability of our model more precisely, we have tried to describe the change in measured magnetization curves with composition for one system, only by allowing K^* to vary in order to obtain the experimental values for the structural transition, but leaving all other parameters in the Hamiltonian unchanged. We have chosen

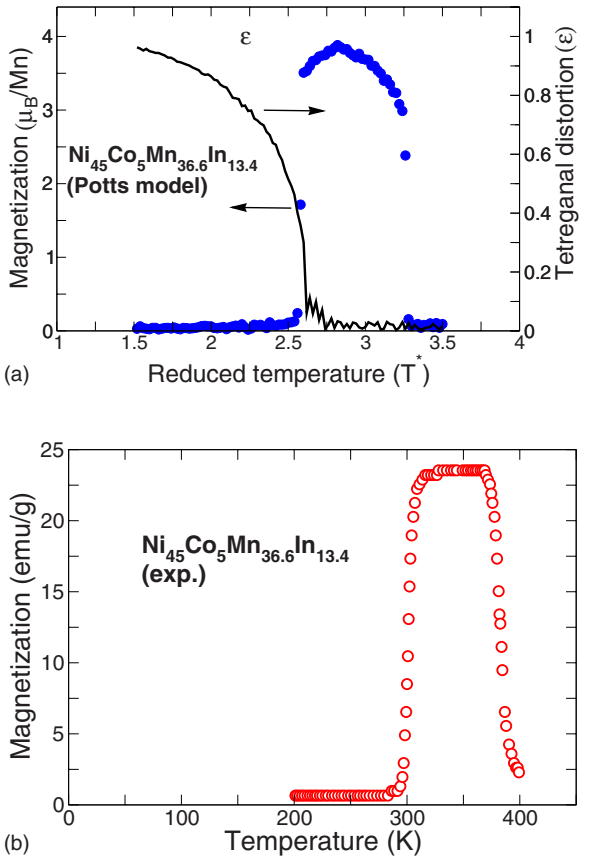

FIG. 9. (Color online) Top panel: Potts model Monte Carlo simulation results of the variation in magnetization (circles) and strain (tetragonal distortion, solid line) as a function of reduced temperature T^* for $Ni_{45}Co_5Mn_{36.6}In_{13.4}$. Lower panel: experimental results taken from Ref. 6.

$Ni_{50}Mn_{25+x}Sb_{25-x}$, for which the magnetization was recently measured for different compositions.[24] As is obvious from Fig. 10, there is some overall agreement with the behavior of the experimental magnetization curves which are shown in Fig. 3.

The corresponding parameters which we adopted for $Ni_{50}Mn_{25+x}Sb_{25-x}$ are listed in Table III. For the alloy series of different compositions x, all parameters have been kept constant except K which has been chosen to reproduce the experimental value of the structural transformation.

More detailed, we estimated the values of $K^*(x)$ from the (T,x)-phase diagram (Fig. 3) so that the values of the theoretical reduced temperature for the structural and AF transitions coincide. For example, for $x=12$ ($x=18$) and $K^*=-0.52$ ($K^*=-130$), the values of the reduced temperatures of the coupled structural and AF transition are approximately equal to 2.3 and 3.0, respectively. In the simulations, the number of lattice sites was taken to be $N=15^3$. The resulting composition-dependent theoretical and experimental magnetization curves show some qualitative agreement; compare Figs. 3 and 10.

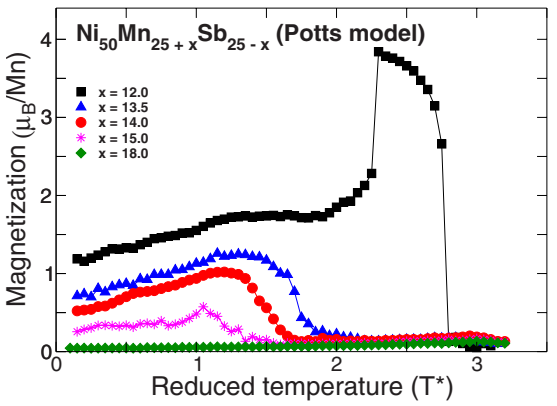

FIG. 10. (Color online) Theoretical variation in magnetization as a function of the reduced temperature T^* in $Ni_{50}Mn_{25+x}Sb_{25-x}$ for different compositions as obtained from the Monte Carlo simulations.

IV. CONCLUSIONS

In this work, we have investigated the temperature dependence of magnetization and strain of Ni-Mn-X (X=In,Sn,Sb) alloys using Monte Carlo simulations for the Heisenberg and the extended Potts model. In the latter case the spin moments of Mn interact on a simple-cubic lattice with coordination $z=6$; here, part of the Mn atoms are assumed to interact only antiferromagnetically, whereby the concentration of these Mn atoms is determined by the experimental composition of $Ni_{50}Mn_{25+x}X_{25-x}$. In addition to the magnetic interactions, the model Hamiltonian contains structural degrees of freedom allowing for a tetragonal deformation. The magnetic subsystem is described by the q-state Potts model. For the structural subsystem, we have used the degenerated Blume-Emery-Griffiths model. The resulting model allows for a combined magnetostructural phase transition of the first order. The antiferromagnetic interaction term in the model leads to several magnetic phase transitions

TABLE III. Model parameters in meV used in the Potts model Monte Carlo simulations of $Ni_{50}Mn_{25+x}Sb_{25-x}$ in an external magnetic field of $H_{ext}=1$ kOe (see Fig. 10).

	J	J_{fm}	J_{afm}	U	K	T_{afm}
$Ni_{50}Mn_{37}Sb_{13}$	1.74	4.44	3.92	−1.57	−0.52	2.33
$Ni_{50}Mn_{38.5}Sb_{11.5}$	1.74	4.44	3.92	−1.57	−2.61	2.33
$Ni_{50}Mn_{39}Sb_{11}$	1.74	4.44	3.92	−1.57	−5.39	2.33
$Ni_{50}Mn_{40}Sb_{10}$	1.74	4.44	3.92	−1.57	−26.9	2.33
$Ni_{50}Mn_{43}Sb_{7}$	1.74	4.44	3.92	−1.57	−130	2.33

from the high-temperature paramagnetic phase to different magneto-ordered phases with decreasing temperature such as the ferromagnetic phase, the antiferromagnetic phase, or a mixed ferro/antiferromagnetic phase. The corresponding temperatures of these phase transitions are determined by the competition of ferromagnetic and antiferromagnetic exchange constants. The degenerated BEG model allows to describe the transition from the high-temperature cubic (austenitic) phase to the low-temperature tetragonal (martensitic) phase. In each alloy case, the experimental value of the martensitic transformation temperature T_m has been taken as a main fitting parameter, although, in general, the parameter values used in the Potts model Monte Carlo simulations are not too far off from corresponding *ab initio* values.

The comparison of results of simulations and experiment is satisfying, in spite of the fact that a fully self-consistent *ab initio* kind of treatment as well as the use of the actual complex lattice of four interpenetrating fcc lattices still need to be undertaken. We also expect that the model Hamiltonian may successfully be used in the investigation of the magnetic shape memory and the magnetocaloric effect.

A final remark concerns the usefulness of the present model to predict different magnetic Heusler alloys which are better suited for applications due to higher Curie and martensitic transition temperatures. In particular, for magnetocaloric devices one would need the magnetostructural transition to occur around room temperature. It is obvious from the simulation of the Co-based system shown in Fig. 8 that this is indeed possible and a close look at Table II allows also speculations about what parameters should be changed in order to achieve better alloys of technological relevance. However, we would also like to point out that this kind of combinatorial materials research can only be achieved by hand in hand laborious *ab initio* calculations. How subtle changes in the composition, in this case the addition of Co, might change the finite-temperature materials parameters have been discussed in Ref. 48. Another promising route which we have started is using *ab initio* calculations for binary transition-metal alloys which show metamagnetic and martensitic tendencies such as Fe-Mn, Fe-Ni, Ni-Mn, Fe-Pd, and Fe-Pt and subsequently optimizing the alloy properties by adding a third element; see, for instance, the work in Ref. 49. *Ab initio* calculations along these lines have been started. In this context, accompanying model calculations as in this paper might help obtain suggestions for combining different materials in an optimal way without doing tedious *ab initio* calculations for each case.

ACKNOWLEDGMENTS

This work was supported by RFBR under Grants No. 06-02-16266, No. 07-02-96029-r-ural, No. 06-02-39030-NNSF, and No. 07-02-13629-OFI-ts, Human Capital, and the DFG through Grant No. SPP 1239, Change of microstructure and shape of solid materials by external magnetic fields. We thank Mehmet Acet for discussions regarding the experimental $M(T)$ plots.

[1] P. Entel, V. D. Buchelnikov, M. E. Gruner, A. Hucht, V. V. Khovailo, S. K. Nayak, and A. T. Zayak, Mater. Sci. Forum **583**, 21 (2008).
[2] O. Söderberg, A. Sozinov, Y. Ge, S.-P. Hannula, and V. K. Lindroos, in *Handbook of Magnetic Materials*, edited by J. Buschow (Elsevier, Amsterdam, 2006), Vol. 16.
[3] M. Khan, A. Pathak, M. Paudel, I. Dubenko, S. Stadler, and N. Ali, J. Magn. Magn. Mater. **320**, L21 (2008).
[4] Z. D. Han, D. H. Wanga, C. L. Zhang, S. L. Tang, B. X. Gu, and Y. W. Du, Appl. Phys. Lett. **89**, 182507 (2006).
[5] J. Cui, Y. S. Chu, O. O. Famuda, Y. Furuya, J. Hattrick-Simpers, R. D. James, A. Ludwig, S. Thienhaus, M. Wuttig, Z. Zhang, and I. Takeuchi, Nature Mater. **5**, 286 (2006).
[6] R. Kainuma, Y. Imano, W. Ito, Y. Sutou, H. Morito, S. Okamoto, O. Kitakami, K. Oikawa, A. Fujity, T. Kanomata, and K. Ishida, Nature (London) **439**, 957 (2006).
[7] R. Kainuma, Y. Imano, W. Ito, H. Morito, Y. Sutou, K. Oikawa, A. Fujity, K. Ishida, S. Okamoto, O. Kitakami, and T. Kanomata, Appl. Phys. Lett. **88**, 192513 (2006).
[8] T. Krenke, E. Duman, M. Acet, E. F. Wassermann, X. Moya, Ll. Mañosa, A. Planes, E. Suard, and B. Ouladdiaf, Phys. Rev. B **75**, 104414 (2007).
[9] T. Krenke, E. Duman, M. Acet, E. F. Wassermann, X. Moya, Ll. Mañosa, and A. Planes, Nature Mater. **4**, 450 (2005).
[10] V. V. Khovaylo, K. P. Skokov, Y. S. Koshkidko, V. V. Koledov, V. G. Shavrov, V. D. Buchelnikov, S. V. Taskaev, H. Miki, T. Takagi, and A. N. Vasiliev, Phys. Rev. B **78**, 060403(R) (2008).
[11] Y. Sutou, Y. Imano, N. Koeda, T. Omori, R. Kainuma, K. Ishida, and K. Oikawa, Appl. Phys. Lett. **85**, 4358 (2004).
[12] E. Şaşıoğlu, L. M. Sandratskii, and P. Bruno, Phys. Rev. B **77**, 064417 (2008).
[13] E. Şaşioğlu, L. M. Sandratskii, P. Bruno, and I. Galanakis, Phys. Rev. B **72**, 184415 (2005).
[14] E. Şaşıoğlu, L. M. Sandratskii, and P. Bruno, Phys. Rev. B **71**, 214412 (2005).
[15] E. Şaşıoğlu, L. M. Sandratskii, and P. Bruno, Phys. Rev. B **70**, 024427 (2004).
[16] J. Rusz, L. Bergqvist, J. Kudrnovský, and I. Turek, Phys. Rev. B **73**, 214412 (2006).
[17] Y. Kurtulus, R. Dronskowski, G. D. Samolyuk, and V. P. Antropov, Phys. Rev. B **71**, 014425 (2005).
[18] This is only correct in the spirit of a model Hamiltonian with effective magnetic exchange parameters taken from *ab initio* calculations as in this paper, where smaller exchange interactions may be neglected for simplicity. For a more detailed discussion of the competition between Ruderman-Kittel-Kasuya-Yoshida-type ferromagnetic and *sp*-electron-mediated antiferromagntic superexchange interactions depending on composition, band filling and resulting details of the electronic spectrum of the magnetic Heusler alloys, see Ref. 12.
[19] H. Akai and P. H. Dederichs, Phys. Rev. B **47**, 8739 (1993); H. Akai, http//sham.phys.sci.osaka-u.ac.jp/kkr/

[20] M. Ogura, A. Hucht, M. E. Gruner, H. Akai, P. Entel, and V. D. Buchelnikov (unpublished), KKR-CPA data.
[21] A. I. Liechtenstein, M. I. Katsnelson, V. P. Antropov, and V. A. Gubanov, J. Magn. Magn. Mater. **67**, 65 (1987).
[22] M. Khan, I. Dubenko, S. Stadler, and N. Ali, J. Appl. Phys. **102**, 113914 (2007).
[23] M. Khan, I. Dubenko, S. Stadler, and N. Ali, Appl. Phys. Lett. **91**, 072510 (2007).
[24] M. Khan, I. Dubenko, S. Stadler, and N. Ali, J. Phys.: Condens. Matter **20**, 235204 (2008).
[25] V. D. Buchel'nikov, S. V. Taskaev, M. A. Zagrebin, and P. Entel, JETP Lett. **85**, 560 (2007).
[26] V. D. Buchelnikov, S. V. Taskaev, M. A. Zagrebin, and P. Entel, Mater. Sci. Forum **583**, 131 (2008).
[27] S. Narasimhan and S. de Gironcoli, Phys. Rev. B **65**, 064302 (2002).
[28] F. Körmann, A. Dick, B. Grabowski, B. Hallstedt, T. Hickel, and J. Neugebauer, Phys. Rev. B **78**, 033102 (2008).
[29] R. B. Potts, Proc. Cambridge Philos. Soc. **48**, 106 (1952).
[30] B. Nienhuis, E. K. Riedel, and M. Schick, Phys. Rev. B **23**, 6055 (1981).
[31] M. Blume, V. J. Emery, and R. B. Griffith, Phys. Rev. A **4**, 1071 (1971).
[32] T. Krenke, M. Acet, E. F. Wassermann, X. Moya, Ll. Mañosa, and A. Planes, Phys. Rev. B **73**, 174413 (2006).
[33] E. P. Nobrega, N. A. de Oliveira, P. J. von Ranke, and A. Troper, Phys. Rev. B **72**, 134426 (2005).
[34] E. P. Nobrega, N. A. de Oliveira, P. J. von Ranke, and A. Troper, J. Phys.: Condens. Matter **18**, 1275 (2006).
[35] E. P. Nobrega, N. A. de Oliveira, P. J. von Ranke, and A. Troper, J. Appl. Phys. **99**, 08Q103 (2006).
[36] E. P. Nobrega, N. A. de Oliveira, P. J. von Ranke, and A. Troper, Phys. Rev. B **74**, 144429 (2006).
[37] E. P. Nobrega, N. A. de Oliveira, P. J. von Ranke, and A. Troper, Physica B **378-380**, 716 (2006).
[38] E. P. Nobrega, N. A. de Oliveira, P. J. von Ranke, and A. Troper, J. Magn. Magn. Mater. **310**, 2805 (2007).
[39] T. Castan, E. Vives, and P.-A. Lindgard, Phys. Rev. B **60**, 7071 (1999).
[40] A. Zheludev, S. M. Shapiro, P. Wochner, A. Schwartz, M. Wall, and L. E. Tanner, Phys. Rev. B **51**, 11310 (1995).
[41] A. Zheludev, S. M. Shapiro, P. Wochner, and L. E. Tanner, Phys. Rev. B **54**, 15045 (1996).
[42] U. Stuhr, P. Vorderwisch, V. V Kokorin, and P.-A. Lindgard, Phys. Rev. B **56**, 14360 (1997).
[43] F. Y. Wu, Rev. Mod. Phys. **54**, 235 (1982).
[44] C. Choi and J. Kim, J. Korean Phys. Soc. **46**, 562 (2005).
[45] P.-A. Lindgard, Phys. Rev. B **60**, 12504 (1999).
[46] D. P. Landau and K. Binder, *A Guide to Monte Carlo Simulations in Statistical Physics* (Cambridge Univesity Press, Cambridge, 2000).
[47] A. K. Pathak, M. Khan, I. Dubenko, S. Stadler, and N. Ali, Appl. Phys. Lett. **90**, 262504 (2007).
[48] P. Entel, M. E. Gruner, W. A. Adeagbo, and A. T. Zayak, Mater. Sci. Eng., A **481-482**, 258 (2008).
[49] J. Buschbeck, I. Opahle, S. Fähler, L. Schultz, and M. Richter, Phys. Rev. B **77**, 174421 (2008).